Heat Treatment Effect on Hydrogen Permeation and Trapping in the API 5CT P110 Steel

M. S. Oliveira[a] [ID] **, J. A. P. Carrasco[b]*** [ID] **, E. O. Vilar[c]** [ID] **, R. C. O. Duarte[c]** [ID] **,**

M. A. dos Santos[a], A. A. Silva[a] [ID] **, L. H. Carvalho[a]** [ID]

[a]*Universidade Federal de Campina Grande, Unidade Acadêmica de Engenharia Mecânica, Campina Grande, PB, Brasil.*
[b]*Universidade Federal de Pernambuco, Departamento de Engenharia Mecânica, Recife, PE, Brasil.*
[c]*Universidade Federal de Campina Grande, Unidade Acadêmica de Engenharia Química, Campina Grande, PB, Brasil.*

The effect of heat treatment on hydrogen diffusion and trapping on the API 5CT P110 steel was investigated trough electrochemical permeation tests and microstructural analysis techniques. Samples of as-received steel were tempered at different temperatures to obtain hydrogen permeation and trapping parameters and to characterize microstructural modifications that may alter these parameters. After permeation tests on each heat-treatment condition were verified changes on hydrogen kinetic parameters. Microstructural analysis revealed changes in dislocations density and volumetric fraction of titanium carbides, responsible to alterations in diffusivity, solubility and in hydrogen trapping characteristics. As these carbides are considered irreversible hydrogen traps, are beneficial because they become the steels less susceptible to hydrogen embrittlement. Therefore, the results suggest that there is an optimal tempering temperature which can make the API 5CT P110 steel more resistant against hydrogen embrittlement, since promote the formation of a higher number of irreversible hydrogen traps.

Keywords: *API 5CT P110 steel, hydrogen embrittlement, hydrogen trapping density, heat treatment.*

1. Introduction

The offshore oil industry is challenging. During operations, the structures used are susceptible to environmental factors such as the high corrosion potential caused by chlorides in seawater, microbial activities due to the characteristics of the fluids conducted, which sometimes contain H_2S etc. These factors can, jointly or individually, lead to failures. Corrosion processes are highly harmful to steel structures, but they can be avoided by using cathodic protection systems, widely used in offshore oil industry. When cathodic protection is used, the structures are cathodically polarized, reactions involving oxygen reduction, Equation 1, and water dissociation, Equation 2, occurs on the auxiliary electrode and the protected part respectively.

$$O_2 + 2H_2O + 4e^- \rightarrow 4OH^- \tag{1}$$

$$2H_2O + 2e^- \rightarrow H_2 + 2OH^- \tag{2}$$

However, when the electric current density produced by these systems is too high, the so-called cathodic overprotection occurs, and substantial amounts of hydrogen atoms are produced at the coating defects. The hydrogen generated by the cathodic protection accumulates on the surface of the steel, later diffuses in the form of atomic hydrogen into the lattice and is trapped in microstructural heterogeneities, called hydrogen traps, thus giving rise to so-called hydrogen trapping[1].

When a load is applied, the hydrogen trapped on trapping sites moves to the highly stressed sites where it can generate degradation processes, as hydrogen embrittlement[2,3]. This degradation process can affect the mechanical properties of steels, with effects such as reduced strength, reduced ductility, and the occurrence of brittle fracture.

Hydrogen traps are classified as reversible and irreversible, according to their binding energy and hydrogen-holding capacity. Traps are considered reversible when their binding energy is less than 60 kJ/mol, such as grain boundaries and dislocations; as the hydrogen atoms retained in these traps can easily abandon them, can also be considered as a mobile or diffusible hydrogen. Traps are considered irreversible when their binding energy is greater than or equal to 60kJ/mol, like inclusions and precipitates[4,5]. The quantity and type of traps in material depends on its specific microstructure; in steels, there are usually diverse types of traps that can interact simultaneously with the hydrogen atoms. The main effect of traps is to reduce the hydrogen transport rate through the material[6], and existing research has established that trapping is an important part of hydrogen embrittlement[7] and that hydrogen susceptibility of steels is closely correlated with trapping[8]. Studies on diverse types of steels qualify mobile hydrogen as the most dangerous because it is more easily able to diffuse to crack initiation sites[9,10]. Therefore, the amount of hydrogen trapped on reversible traps has an important effect on the degradation of mechanical properties of steels[11].

*e-mail: jorge.carrasco@ufpe.br

On the other hand, irreversible trapping is considered "beneficial" because hydrogen trapped in these sites do not participate in the embrittlement process[8,9,12]. Currently, it is widely accepted that microstructures with a higher number of irreversible traps are less susceptible to hydrogen effect and that the microstructural manipulation is an effective method to make steels more resistant to hydrogen embrittlement[13,14]. As the susceptibility to hydrogen embrittlement is strongly affected by the material's microstructure, although environmental factors are also very important[3], understanding microstructural factors is essential to define metallurgical processes that reduce the susceptibility of steels against hydrogen embrittlement and other-hydrogen degradation processes.

Thermal and mechanical processes can modify the microstructure and change the mechanical properties of steels, affecting their susceptibility to hydrogen embrittlement due to the formation of new irreversible trapping sites[15]. Microstructure modification of steels used in oil pipelines is a technique used extensively to increase their resistance to hydrogen embrittlement[16-19]. This is done by controlling parameters involved in thermomechanical processes, such as cooling rate, rolling and heating temperatures. Tempering is a heat treatment used to stress relieving developed in quenching processes and also to increase the mechanical strength or the toughness of the treated material. It can run over a wide range of temperatures, depending on the changing of the property targeted by the treatment[20,21].

Although many studies have been performed on the development of steels resistant to hydrogen embrittlement, results show that more work still needs to be done, such as verify the effect of heat treatment parameters on microstructure optimization and the mechanical properties of materials. The API 5CT P110 steel is a high strength and low alloy (HSLA) steel used in the manufacturing of casing pipes and couplings for oil wells, which started to be used to manufacture tubing and casing for risers in view of their excellent combination of good fracture toughness and high mechanical strength[6]. This steel follows the API 5CT standard classification[22], which does not specify the composition of carbon and alloy elements for grade P110; only the S and P contents are specified, which depend on the process used in the manufacture of the tube. The main requirement of the standard is that the tubes manufactured with this steel be heat treated by a quenching and tempering process. In this way, during the factory production stage the tubes manufactured with this steel according to the API 5CT standard receive a first heat treatment in the industrial plant.

Despite the application of this steel in riser tubes carry new challenges associated with the need for cathodic protection and the nature of the transported fluids, because hydrogen damage processes can be generated, there is little information on the scientific literature about studies related to the changes on hydrogen diffusivity and trapping due to heat treatments[23,24].

The electrochemical permeation test, based on the technique developed by Devanathan and Stachursky[25] it is widely used to study hydrogen diffusion and hydrogen trapping in different materials[16,26]. This technique was used here to investigate the effect of tempering heat treatment on hydrogen diffusion and hydrogen trapping in API 5CT P110 steel, as well as their correlation with the microstructural changes that can modify their hydrogen embrittlement susceptibility.

2. Materials and Methods

This study was performed using the API 5CT P110 steel, supplied in the form of seamless pipe gutter, with 330mm outer diameter and 14mm wall thickness, provided by the CENPES/PETROBRAS. The chemical composition determined by optical emission spectrometer analysis is displayed in Table 1.

In order to determine the hydrogen kinetic parameters and hydrogen trapping characteristics of the studied steel, potentiodynamic polarization and permeation tests were performed, first on samples of as-received steel and after on samples of steel tempered at three different temperatures. The microstructure resulting from the heat treatments was characterized, as well as the resulting precipitates.

The metallic membranes for the electrochemical tests were extracted by wire erosion from a pipe wall on rolling direction with 40mm diameter and 1.0mm thickness, according to ASTM G148-97[27]. All samples were first sanded with waterproof SiC papers, grade 120, 320, 600, 1000 and 1200, to remove surface irregularities and oxides, and then polished with alumina in suspension, with granulometry of 0.05 μm, 0.3 μm and 1 μm. The area exposed to the electrolyte was 3.14mm[2]. A schematic of samples is show in Figure 1.

Before starting electrochemical tests, one part of the metallic membranes of as-received steel was quenched to 870[0]C and cooled in water, at a cooling rate of 50[0]C/s. Then, the quenched steel samples were shared into three groups and the samples of each group were tempered, in a simple tempered process, to same temperature.
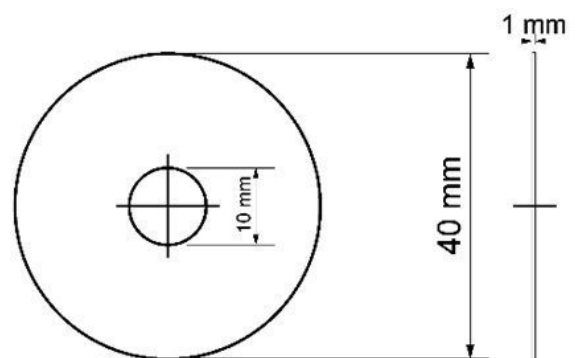

Figure 1. Schematic of samples used in electrochemical tests[27].

Table 1. Chemical composition (% weight) of API 5CT P110 steel.

C	Si	Mn	P	S	Ni	Cr	Cu	Mo	Al	V	Ti	Fe
0.284	0.242	1.085	0.010	0.006	0.019	0.294	0.002	0.136	0.044	0.006	0.030	Balance

The samples of 1st. group were tempered to 350°C, the samples of 2nd. group to 440°C and the samples of 3rd. group to 525°C. In all cases, the heat time was 30 min. The codes T350, T440 and T525 were assigned to the three conditions, respectively. The heat treatments were carried out in an EDG oven, FCVE-II, under an Argon controlled atmosphere using a flow rate of 5l/min and a heating rate of 20⁰C/min.

2.1. Electrochemical tests

The potentiodynamic polarization and hydrogen permeation tests were performed at room temperature (±25°C) in an electrochemical double-cell with a configuration developed by Devanathan and Stachurski[25] described in Figure 2, which consists of two electrochemical cells (charge and detection cells, or input and output cells, respectively) separated by a metallic membrane, according to recommendations of ASTM G148-97 Standard[27].

The potentiodynamic polarization tests were performed using a BioLogic potentiostat model VMP3 with the left cell of electrochemical double-cell filled with a 24g/l NaCl solution, by applying a linear ramp of measured potential against the saturated calomel reference electrode (SCE) at a sweep rate of 0.8 mV/s. A platinum electrode with area of 1 cm² was used as counter electrode. The pH of NaCl solution was adjusted to 8.22 with a 0.1N NaOH solution before starting the tests.

The permeation tests were performed using the two cells of electrochemical double-cell. Hydrogen was produced on the charge cell using the galvanostatic method, and the hydrogen diffused through the sample was oxidized in the detection cell at a potential of $+300mV_{SCE}$. The two-cells were connected to a BioLogic multichannel potentiostat model VMP3, controlled by the Ec-Lab r 11.43 software. The output cell was filled with 0.1M NaOH solution[27] and the input cell with 0.42M of a NaCl solution at pH 8.22 (corrected with NaOH). The hydrogen generation current density used in each test was obtained from the potentiodynamic polarization curves.

The permeation tests were performed to obtain a double transient for each sample. In the first transient, the reversible and irreversible hydrogen traps were filled. Upon reaching the steady-state flow, the hydrogen production was interrupted, and the hydrogen atoms captured in reversible traps were released. After a period of relaxation, the same current intensity was applied, the oxidation current measured and the second transient was obtained.

The apparent diffusion coefficient (D_{app}) to the samples of as-received steel and in the T350, T440 and T525 conditions was calculated by the time-lag (t_l) method through the Equation 3[28,29] using the first transients. The effective diffusivity (D_{eff}) was obtained using the second permeation transients, trough the same equation.

$$D_{app}\left(\text{or } D_{eff}\right) = \frac{L^2}{6t_{lag}} \qquad (3)$$

where L is the sample thickness (cm), t_{lag} (s) is the time required to reach the value of $J(t)/J_\infty$. J_∞ is the atomic hydrogen permeation flux at steady-state[27,30].
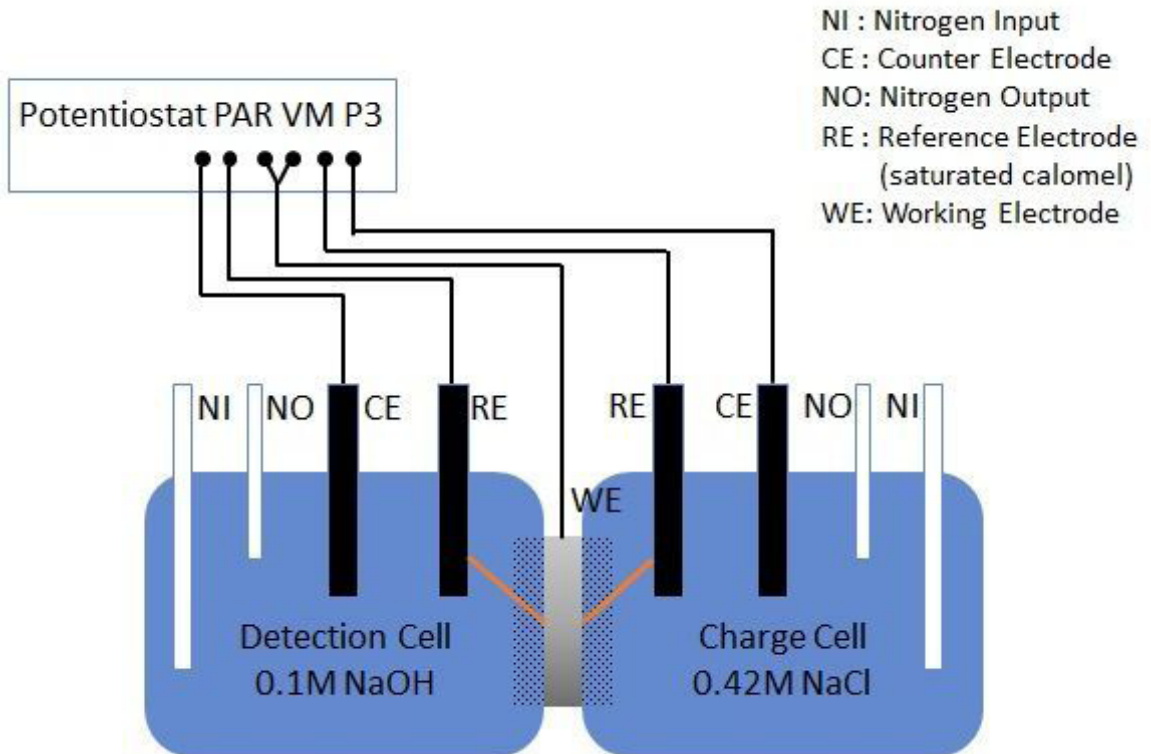

Figure 2. Schematic of double-cell used in electrochemical tests.

The hydrogen solubility on the sample at steady state (apparent solubility), S_{app}, is given by the Equation 4[31] and the hydrogen subsurface concentration on the sample (solubility), C_0, was obtained using the Equation 5[32]:

$$S_{app} = \frac{J_\infty L}{D_{app}} \qquad (4)$$

$$C_0 = \frac{J_\infty L}{D_{eff}} \qquad (5)$$

The total density of hydrogen trapping sites (N_T), when $D_L \gg D_{app}$ ($D_L = 7.2 \cdot 10^{-5} cm^2/s$ is the hydrogen diffusivity in Fe-α)[33] can be determined by the equation proposed by McNabb & Foster[34], Equation 6, using data of first permeation transient. The density of reversible trapping sites (N_r) was calculated from the second permeation transient, taking into account the effective diffusivity (D_{eff}). Finally, the density of irreversible sites (N_i) was obtained by difference among the total density of trapping sites (N_T) and the density of reversible trapping sites (N_r)[35,36].

$$N_T = \frac{J_{ss}L}{D_{app}} N_A \qquad (6)$$

where N_A corresponds to Avogadro's constant.

2.2. Microstructural analysis

Microstructural characterization was performed on samples of as-received steel and of steel at each heat treatment condition. The samples were embedded in bakelite, sanded with waterproof SiC papers, grade 120, 320, 600, 1000 and 1200, and then polished with alumina in suspension, with a granulometry of 0.05 μm, 0.3 μm and 1 μm. After polishing, the samples were cleaned with ethyl alcohol and etched with 2% nitric acid solution (2% Nital). First, a microstructure analysis was performed using a Shimadzu SSX-500 scanning electron microscope. Later, an analysis by energy dispersive spectroscopy to characterize the precipitates existing in the samples was performed.

2.3. X-ray diffraction analysis

In order to identify the present phases on as-received steel and at each heat treatment condition, as well as to determine the density of dislocations, x-ray diffraction measurements were performed with 2Θ ranging from 40º to 140⁰ with CuK$_\alpha$ radiation. This analysis was performed in an X BRUKER, D2 PHASER diffractometer, operating with a Cu target tube at 30.0 kV and 10.0 mA, with a 55D160 detector.

To calculate the dislocation density on as-received steel and on the steel in the three heat treatment conditions, the method proposed by Wllliamson-Hall was used, Equation 7[37].

$$FWHM_{sample} \frac{\cos\theta}{\lambda} = \frac{0,9}{D} + 2\varepsilon \frac{sen\theta}{\lambda} \qquad (7)$$

where FWHM corresponds to half the maximum width, in radians, calculated at different peaks corresponding to the diffraction planes of the ferrite, D is the average grain size and ë the x-ray wavelength (0.15406 nm). FWHM was obtained from diffracted peaks in the (110) (200) (211) planes, which showed a significant change between the diffraction spectra. Equation 8 was used to determine the dislocation density[38-40].

$$p = 14.4 \left(\frac{\varepsilon}{b} \right)^2 \qquad (8)$$

where b represents the burgers vector (b = 0.248 nm) and ε is the slope of the $FWHM_{sample}$ curve on $\frac{\cos\theta}{\lambda}$ Vs $\frac{sen\theta}{\lambda}$ coordinate system[19,41].

3. Results and Discussion

3.1. Potentiodynamic polarization

The potentiodynamic polarization curves of steels in the as-received, T350, T440 and T525 conditions are shown in Figure 3. In the four curves two inflection points can be observed: The point A, at approximately -950mV$_{SCE}$ and the point B, at approximately -1100mV$_{SCE}$.

During the test, the main reduction reaction occurs around the point A, since from this point the increasing production of hydrogen occur according to the reaction represented in Equation 2. At point B, hydrogen production is relatively high, which characterizes a cathodic overprotection condition.

3.2. Hydrogen permeation

The permeation curves were constructed for samples of as-received steel and the steel in T350, T440 and T525 conditions. The current density used in the permeation tests was -3.0mA/cm², that correspond to -1100mV$_{SCE}$ according to the potentiodinamyc polarization curves. This potential was chosen because characterizes a cathodic overprotection condition and the high hydrogen production facilitates the evaluation of the response of material to its effects. In order to facilitate the obtention of the trapping parameters, the permeation curves were plotted in terms of the normalized flux J_{SS}/J and dimensionless time τ ($\tau = \frac{D_L \cdot t}{L^2}$), according to the procedure proposed by Pressouyre and Bernstein[42]. These curves are shown in Figures 4a, 4b, 4c and 4d.

Values for apparent and effective diffusivities, solubility, subsurface concentration and trap density are shown in Table 2.
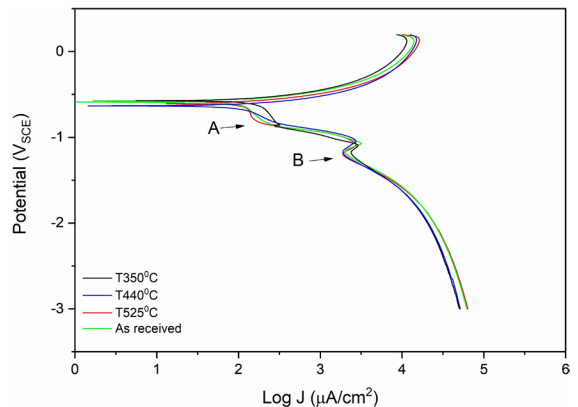

Figure 3. Potentiodynamic polarization curves in NaCl (0.42M), T=25°C.

In Table 2 can be observed that there was an important increase in the hydrogen subsurface concentration after the first heat treatment (T350 condition), followed by a reduction as the temperature used in the heat treatment was increased (T440 and T525 conditions). The behavior of the effective diffusivity was inverse: there was an important decrease on hydrogen diffusion rate trough lattice after the first heat treatment (T350 condition), followed by an increase when the temperature used was 440°C (T440 condition); the increase became expressive at temperature of 525°C (T525 condition). The responsible for alterations on hydrogen transport rate through the material is the hydrogen trapping, since the residence time in traps is greater than the residence time in interstitial lattice sites[6]. Low diffusivity values indicate resistance to hydrogen diffusion through the network[43]. The apparent diffusivity shows the same behavior, but it is lower than the effective diffusivity because the former is obtained when the material is free of hydrogen; in turn, the effective diffusivity is obtained when the irreversible

traps are fully filled. The difference between apparent and effective diffusivity can be attributed to the difference in density of hydrogen traps, such as the volumetric fraction of grain boundaries, dislocations density and precipitates. Increases in grain boundaries, which act as hydrogen trapping sites, tend to reduce hydrogen diffusion[44,45]; the increase on dislocations density also decreases the hydrogen diffusivity[46]. This means that the dislocations are hydrogen traps rather than diffusion paths. The hydrogen solubility is also related to the reversible and irreversible trapping: traps can hold up to 97% of the total hydrogen concentration, which makes them controllers of hydrogen solubility and of the amounts of hydrogen atoms that can be available to diffuse toward to sites where degradation occurs[47,48]. The number of atoms that can be trapped on traps depends on trap characteristics: irreversible traps can have high or limited specific solubility (unsaturable or saturable traps, respectively)[49], reversible traps can be hold very low concentrations of hydrogen atoms, as the case of dislocations[50].
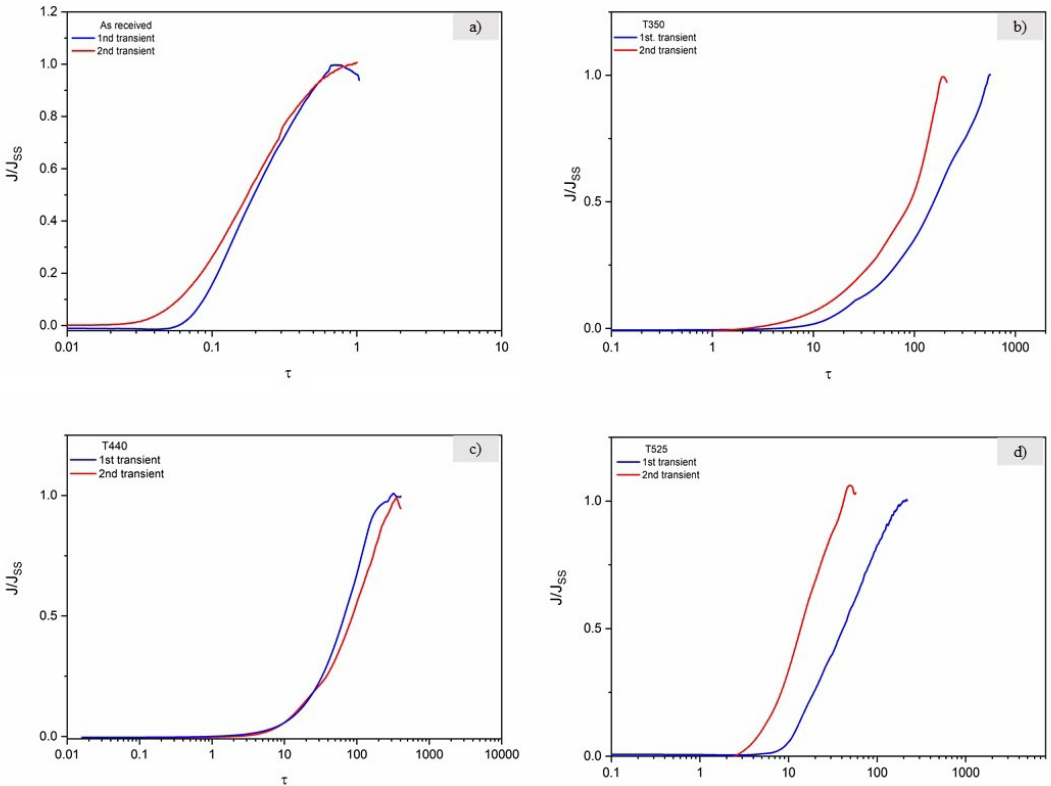

Figure 4. Normalized permeation curves (a) as-received; (b) T350; (c)T440; (d)T525.

Table 2. Kinetic hydrogen parameters obtained in electrochemical permeation tests.

Condition	D_{app} (cm²/s)	D_{eff} (cm²/s)	S_{app} (mol/cm³)	C_0 (mol/cm³)	N_T (sites/cm³)	N_i (sites/cm³)	N_r (sites/cm³)
As-received	$1.32 \cdot 10^{-6}$	$1.65 \cdot 10^{-6}$	$6.51 \cdot 10^{-7}$	$2.95 \cdot 10^{-7}$	$3.92 \cdot 10^{17}$	$2.14 \cdot 10^{17}$	$1.78 \cdot 10^{17}$
T350	$1.58 \cdot 10^{-7}$	$2.83 \cdot 10^{-7}$	$1.05 \cdot 10^{-5}$	$3.62 \cdot 10^{-6}$	$6.32 \cdot 10^{18}$	$4.14 \cdot 10^{18}$	$2.18 \cdot 10^{18}$
T440	$3.00 \cdot 10^{-7}$	$4.07 \cdot 10^{-7}$	$1.02 \cdot 10^{-5}$	$1.64 \cdot 10^{-6}$	$6.15 \cdot 10^{18}$	$5.16 \cdot 10^{18}$	$9.90 \cdot 10^{17}$
T525	$6,12 \cdot 10^{-7}$	$1.67 \cdot 10^{-6}$	$7.98 \cdot 10^{-7}$	$7.29 \cdot 10^{-8}$	$4.80 \cdot 10^{17}$	$4,37 \cdot 10^{17}$	$4.39 \cdot 10^{16}$

Therefore, the differences in the diffusivity and concentration values observed on four conditions (as-received, T350, T440 and T525) are attributed to the formation of new hydrogen trapping sites, reversible and/or irreversible, related to the changes on microstructural characteristics in each condition. The change in tempering temperature leads to modifications in microstructure of material, as changes in grain size, formation of dislocations and precipitates, which, in turn, cause changes in the hydrogen kinetics in the material. For example, the hydrogen solubility is enhanced in smaller grains and the hydrogen transport is difficulted, since trapping by grain boundaries is increased with the decrease in grain size[1,51].

The result of hydrogen trapping quantification shown in Table 2 indicates that, from the as-received condition, there was an increase on total trapping sites density after the first heat treatment at 350ºC (T350 condition), followed to a decrease on total trapping sites density as the temperature on heat treatment was increased (T440 and T525 conditions). This decrease was more expressive in the T525 condition. The reversible and irreversible traps distribution in the total trap density in the three conditions (T350, T440 and T525),

show that the irreversible trapping is more important in T350 and T440 when trapping is associated with the number of atoms trapped in the irreversible traps, that can be obtained calculating the difference between apparent solubility and the subsurface concentration. The results show on Table 2 indicate that the steel on T440 condition presents a microstructure with high solubility, related to its high trapping capacity, and that quantity of hydrogen atoms trapped in the irreversible traps is greater than the as-received, T350 and T525 conditions. These results suggest that the formation of irreversible traps associated with the greater number of hydrogen atoms trapped when the tempering temperature is 440ºC, the heat treatment may make the API 5CT P110 steel less susceptible to hydrogen embrittlement[13,14].

3.3. Microstructure

The microstructural characterization indicated the presence of tempered martensite in all microstructures, Figure 5. This microstructure is composed of laths (blocks), plates and previous austenitic grain boundaries[52].
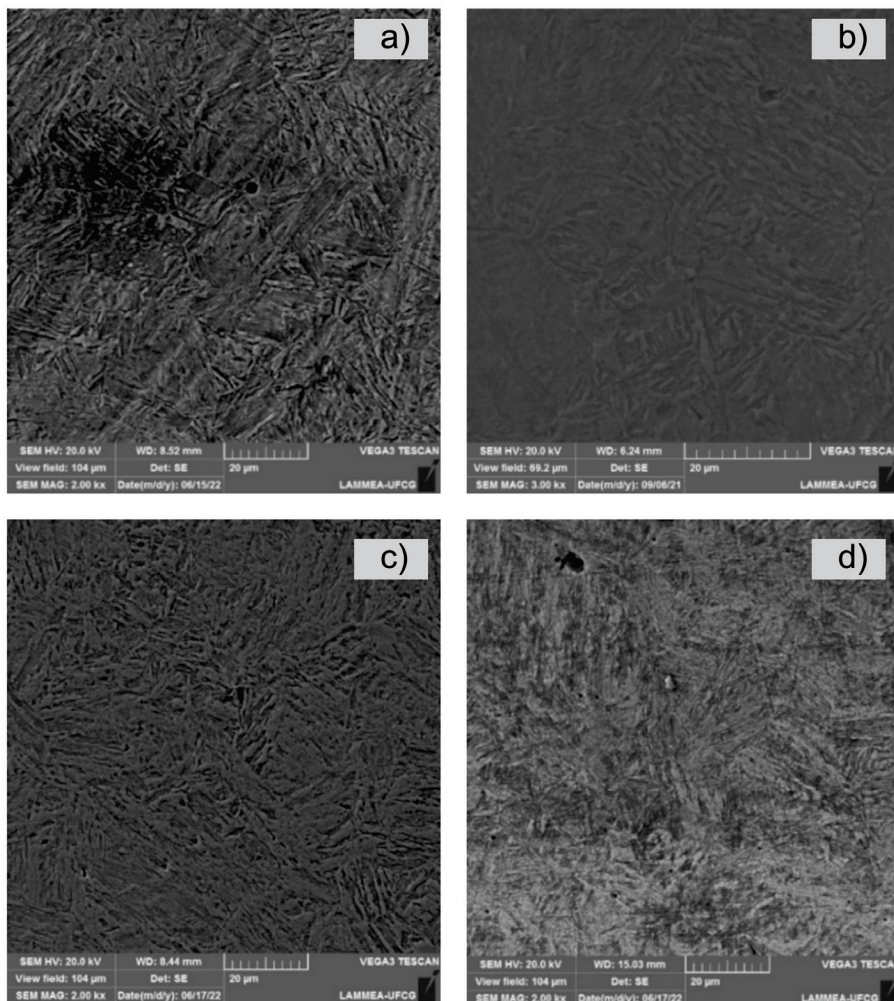

Figure 5. Material microstructure. (a) As-received; (b) T525; (c)T440; (d)T350.

A high dislocation density in martensite is observed on T350, T440 and T525 conditions. Dislocations can be considered as more dangerous trapping sites due to their lower activation energy among other trapping sites[53]. The high dislocation density in martensite hinders the hydrogen transport and reduce the hydrogen diffusivity, therefore, the diffusion coefficient decreases with increasing of dislocation density and the diffusible hydrogen concentration is increased[54]. Despite the effect of dislocations on hydrogen diffusivity, they are not solely responsible for alterations in hydrogen transport rate, which occur due to combined effect of reversible and irreversible trapping.

In order to characterize the hydrogen traps, EDS analysis was performed, Figure 6.
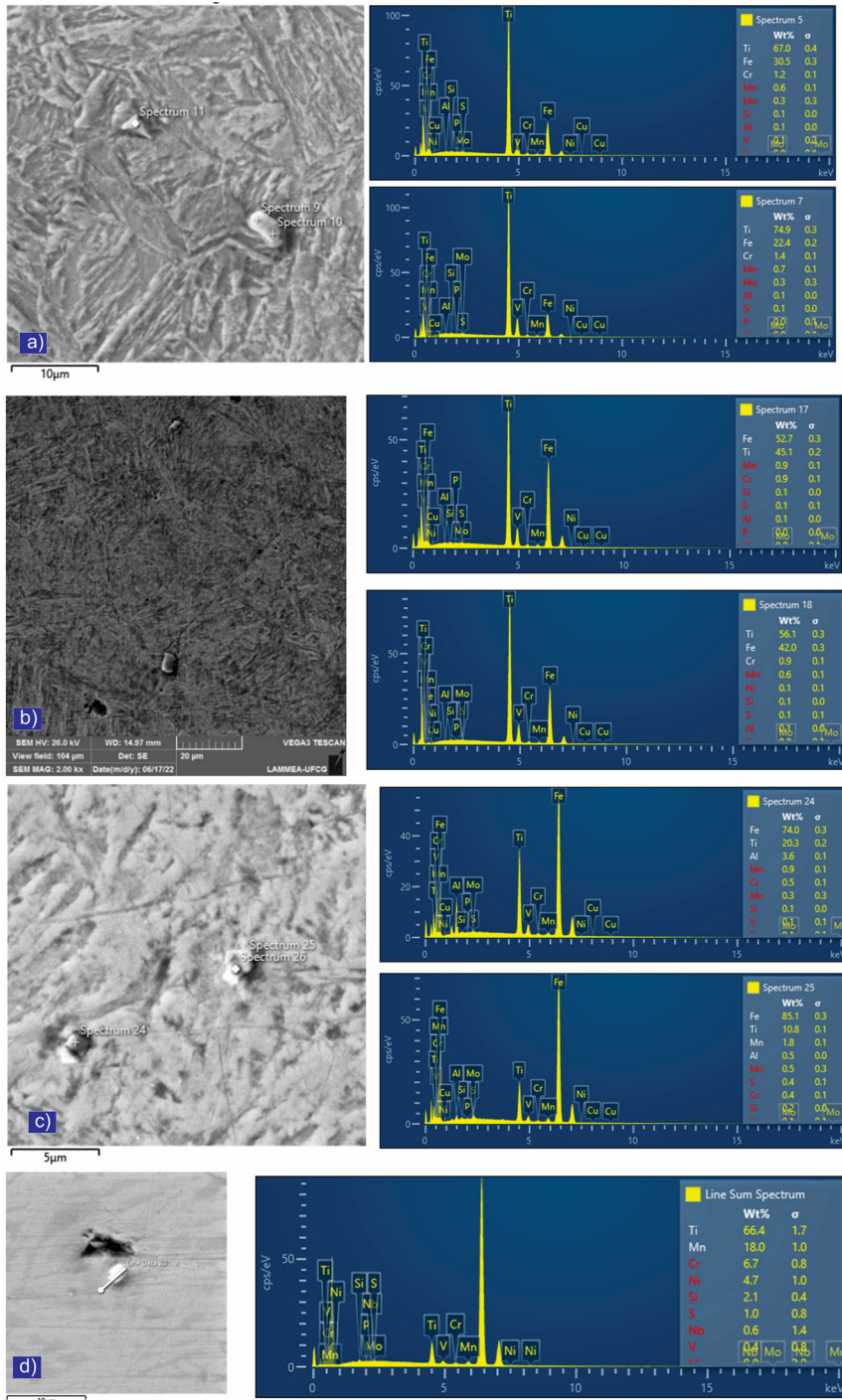

Figure 6. Characterization of precipitates by energy dispersive spectroscopy. (a) As-received; (b) T350; (c) T440; (d) T525.

The different tempering temperatures, induce the precipitation and dissolution of a considerable amount of microalloyed carbonitrides elements. In samples of T350, T440 and T525 conditions, particles containing high levels of Ti, Mn, and Cr were found, which characterize MC, M_3C, M_7C_3, and $M_{23}C_6$ carbides. These carbides are thermodynamically stable in the temperature range between 550°C and 715°C. Ti and Mo are the M constituents of MC-type carbides, while Fe, Cr, Mo, and Mn are the constituents of M_3C, M_7C_3, and $M_{23}C_6$ carbides.

Was observed that the volumetric fraction of M_7C_3 phase gradually decreases until around 600°C, when dissolves completely, while the volumetric fraction of M_3C increases with rising temperature until reaching 730°C, at which point it completely dissolves. The volumetric fraction of MC carbide gradually decreases with the increase of temperature until 460°C, and stars to increase again, reaching a peak between 650°C and 750°C. After this temperature, the fraction starts to decrease. A small fraction of MC precipitate remains until 1200°C. The opposite occurs with $M_{23}C_6$ carbides, which gradually decreases with increasing temperature until it dissolves completely at around 650°C. Yang[55] studied the API 5CT P110 steel under different heat treatments and found similar results. The average particle sizes under the four conditions are presented in Table 3.

The reduction in particle size was significant at 440°C. The reduction from 3.47 μm in T350 to 1.07 μm in T440 condition was due to the decrease in the volumetric fraction of M_7C_3 and $M_{23}C_6$ carbides. Analysis of Figure 5 showed a high content of Cr in the sample tempered at 350°C, but this element was not found in the samples tempered at 440°C and 525°C. Additionally, there was an increase in the average particle size between 440°C and 525°C (1.07 ± 0.22 and 1.11 ± 0.14, respectively). However, a more in-depth analysis, considering the standard deviations, revealed that there is no statistically significant difference in the average particle size within the margin of error between the two temperatures. Interestingly, the samples treated at 440°C consistently exhibited a larger average particle size, falling within the measurement error range when compared to the particles treated at 525°C

With the increase in tempering temperature, there is a dissolution of M_7C_3 and $M_{23}C_6$ precipitates in the steel, resulting in a significant reduction in the number of reversible trapping sites, which is evidenced by the reduction in the density of reversible hydrogen trapping sites with increasing of tempering temperature. As the M7C3 (Cr) carbides have a low activation energy to release hydrogen, and are considered reversible traps[56,57], the continuous increase in apparent diffusivity is also related to this reduction.

Particle refinement was possible to observe on sample of T440 condition. The effect of-observed refinement on the apparent diffusivity was most evident in the T525 condition, where the irreversible trapping sites density was higher than the reversible trapping sites, when compared to the T440 condition. It is believed that this can be explained by the secondary precipitation of Ti-rich MC-type carbides. The apparent diffusivity was higher on T440 and T525 conditions due to the smaller size of the carbide.

TiC-type precipitates introduced by tempering are, therefore, beneficial because of their potential as hydrogen capture sites. These traps are characterized as irreversible traps[42,58]. Wei and Tsuzaki studied the effect of TiC on a 0.05C-0.22Ti-2.0Ni steel, obtaining the energy for hydrogen desorption from this precipitate around 85.7 kJ/mol, which characterizes a strong irreversible trapping site. Furthermore, Pressouyre and Bernstei[42] and Lee and Lee[59] reported that the activation energy increased with the size of the precipitate. According to the D_{app} values, this value increases as the second phase (TiC) particle size decreases. Precipitated particles of (Nb,Ti)C present a greater capacity to capture hydrogen than (Cr,Mo)xCy precipitates due to their greater affinity by hydrogen[60,61].

3.4. XRD analysis

The profiles of the x-ray diffraction lines are shown in Figure 7. The observed peaks in each phase have the same reflection in the range of 40-140^0 for the planes (1 1 0) (2 0 0) (2 1 1) (2 2 0) (3 1 0) (2 2 2), which correspond to the α' ferrite phase. The absence of austenite peaks in the diffraction spectra indicates a structure quasi 100% BCC-α'-Fe without significant content of retained austenite[62]. Peaks (110) (200) (211) of martensite shifted to the right, while peaks (220) (310) (222) remained practically unchanged[63]. The shift to the right of the first three peaks may be due to carbon diffusion during the tempering process. The dislocation density as a function of tempering temperature is shown in Figure 8.

The density of dislocations in the as-received, T350, T440 and T525 conditions was $1.13 \cdot 10^{12}$ cm^{-2}, $1.68 \cdot 10^{12}$ cm^{-2}, $1.67 \cdot 10^{12}$ cm^{-2} and $1.40 \cdot 10^{12}$ cm^{-2}, respectively. As observed, the tempering reduced the dislocations density. The minimum value for dislocation density was obtained for the material in the as-received condition. This steel, during manufacturing stages, underwent heat treatment involving quenching and tempering with different conditions than those studied in this work, such as the furnace holding time and tempering temperature, which are fundamental parameters influencing dislocation density[64].

Table 3. Average size of particles.

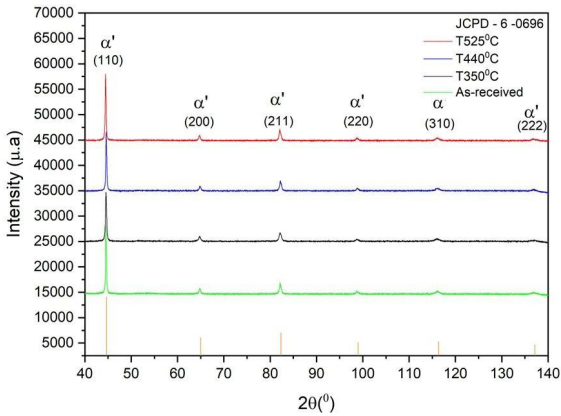| Condition	Average size of particles (μm)
As-received	1.90 ± 0.32
T350	3.47 ± 1.29
T440	1.07 ± 0.22
T525	1.11 ± 0.14

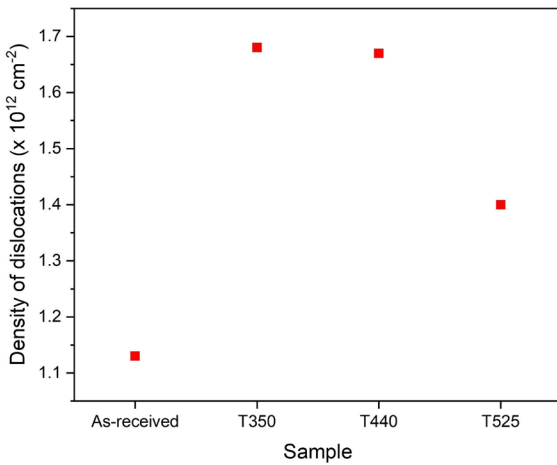**Figure 7.** API 5CT P110 steel diffractogram.

Figure 8. Density of dislocations as a function of tempering temperature.

4. Conclusions

In this work the diffusivity and hydrogen trapping in API 5CT P110 steel tempered at different temperatures were characterized experimentally by the electrochemical permeation technique[25], as well as was established the effect of heat treatments in microstructural changes responsible for alterations on kinetic hydrogen parameters on the studied steel. The following findings can be drawn from permeation experimental results and from microstructural characterization:

a) The heat treatments caused significant changes in the hydrogen diffusion and hydrogen solubility. There was an increase in the hydrogen transport rate with the increase in tempering temperature, in the following order: T350 < T440 < T525. The behavior of the hydrogen concentration was inverse, there was a decrease in solubility with increasing in the heat treatment temperature.

b) These differences in the diffusivity and solubility values are attributed to the formation of new hydrogen trapping sites, reversible and/or irreversible, related to the changes on microstructural characteristics in the different tempering temperatures.

c) There was a reduction in the dislocation density between 350ºC and 525ºC and a significant reduction in the average particle size until 440°C followed to an increase until 525ºC. The reduction in the average particle size was attributed to the decrease in the volumetric fraction of M7C3 and M23C6 carbides. The increase was attributed to the increase in the volumetric fraction of MC-type carbides.

d) The MC-type carbides, rich in Ti, are irreversible hydrogen traps because can trap large amounts of hydrogen atoms with high trapping energy. As larger their size, more hydrogen atoms can trap. Therefore, are considered beneficial taps.

The results indicate that the presence of stable carbides and the controlled particle size distribution in the microstructure of API 5CT P110 steel, obtained through optimized heat treatments, can improve their hydrogen retention capacity, and can make it less susceptible to hydrogen embrittlement, reducing, therefore, the risk of catastrophic failures. The results suggest that the optimal tempering temperature is 440ºC, according to the conditions outlined for the studied problem. These conclusions have important implications, especially in critical applications in the oil and gas industry, where cathodic protection systems are used.

5. Acknowledgments

6. References

1. Krom AHM, Bakker A. Hydrogen trapping models in steel. Metall Mater Trans, B, Process Metall Mater Proc Sci. 2000;31(6):1475-82. http://dx.doi.org/10.1007/s11663-000-0032-0.

2. Villalobos JC, Serna SA, Campillo B, López-Martínez E. Evaluation of mechanical properties of an experimental microalloyed steel subjected to tempering heat treatment and its effect on hydrogen embrittlement. Int J Hydrogen Energy. 2017;42(1):689-98.

3. Valentini R, Solina A, Tonelli L, Lanza S, Benamati G, Donato A. Reversible and irreversible hydrogen trapping in metals: new computer-based code THYDA. J Nucl Mater. 1996;233-237:1123-7.

4. Rivera PC, Ramunni VP, Bruzzoni P. Hydrogen trapping in an API 5L X60 steel. Corros Sci. 2012;54:106-18.

5. Huang F, Liu J, Deng ZJ, Cheng JH, Lu ZH, Li XG. Effect of microstructure and inclusions on hydrogen induced cracking susceptibility and hydrogen trapping efficiency of X120 pipeline steel. Mater Sci Eng A. 2010;527(26):6997-7001.

6. Jemblie L, Olden V, Akselsen OM. A coupled diffusion and cohesive zone modelling approach for numerically assessing hydrogen embrittlement of steel structures. Int J Hydrogen Energy. 2017;42(16):11980-95. http://dx.doi.org/10.1016/j.ijhydene.2017.02.211.

7. Taha A, Sofronis P. A micromechanics approach to the study of hydrogen transport and embrittlement. Eng Fract Mech. 2001;68(6):803-37. http://dx.doi.org/10.1016/S0013-7944(00)00126-0.

8. Tsay LW, Chi MY, Wu YF, Wu JK, Lin D-Y. Hydrogen embrittlement susceptibility and permeability of two ultra-high strength steels. Corros Sci. 2006;48(8):1926-38. http://dx.doi.org/10.1016/j.corsci.2005.05.042.

9. Chun YS, Kim JS, Park K-T, Lee Y-K, Lee CS. Role of ε martensite in tensile properties and hydrogen degradation of high-Mn steels. Mater Sci Eng A. 2012;533:87-95. http://dx.doi.org/10.1016/j.msea.2011.11.039.

10. Scully JR, Dogan H, Li D, Gangloff RP. Controlling hydrogen embrittlement in ultra-high strength steels. In: Corrosion; 2004; New Orleans, Louisiana,. Proceedings. Houston: NACE; 2004. (Paper 04563).

11. Takai K, Watanuki R. Hydrogen in trapping states innocuous to environmental degradation of high-strength steels. ISIJ Int. 2003;43(4):520-6.

12. Tsay LW, Hu YF, Chen C. Embrittlement of T-200 maraging steel in a hydrogen sulfide solution. Corros Sci. 2005;47(4):965-76. https://doi.org/10.1016/j.corsci.2004.06.017.

13. Luppo MI, Ovejero-Garcia J. The influence of microstructure on the trapping and diffusion of hydrogen in a low carbon steel. Corros Sci. 1991;32(10):1125-36. http://dx.doi.org/10.1016/0010-938X(91)90097-9.

14. Maroef I, Olson DL, Eberhart M, Edwards GR. Hydrogen trapping in ferritic steel weld metal. Int Mater Rev. 2002;47(4):191-223. http://dx.doi.org/10.1179/095066002225006548.

15. Marchetti L, Herms E, Laghoutaris P, Chêne J. Hydrogen embrittlement susceptibility of tempered 9%Cr-1%Mo steel. Int J Hydrogen Energy. 2011;36(24):15880-7. http://dx.doi.org/10.1016/j.ijhydene.2011.08.096.

16. Pourazizi R, Mohtadi-Bonab MA, Davani RKZ, Szpunar JA. Effect of thermo-mechanical controlled process on microstructural texture and hydrogen embrittlement resistance of API 5L X70 pipeline steels in sour environments. Int J Press Vessels Piping. 2021;194:104491. http://dx.doi.org/10.1016/j.ijpvp.2021.104491.

17. Nagu GA, Amarnath, Namboodhiri TKG. Effect of heat treatments on the hydrogen embrittlement susceptibility of API X-65 grade line-pipe steel. Bull Mater Sci. 2003;26(4):435-9. http://dx.doi.org/10.1007/BF02711189.

18. Prasad PS, Ghosh KS. Effect of heat treatment and NC Ni coating on electrochemical and hydrogen embrittlement behaviour of a High Strength Low Alloy (HSLA) Steel. Electrocatalysis. 2022;13(5):551. http://dx.doi.org/10.1007/s12678-022-00744-4.

19. Zhang D, Li W, Gao X, Fu L, Guo J, Zhang J, et al. Effect of cold deformation before heat treatment on the hydrogen embrittlement sensitivity of high-strength steel for marine risers. Mater Sci Eng A. 2022;845:143220. http://dx.doi.org/10.1016/j.msea.2022.143220.

20. Thelning K-E. Steel and its heat treatment. London: Butterworth-Heinemann; 2013

21. Chiaverini V. Aços e ferros fundidos. São Paulo: ABM; 1977;

22. API: American Petroleum Institute. API specification 5CT: specification for casing and tubing. 9th ed. Washington, DC: API; 2011.

23. Simoni L, Caselani JQ, Ramos LB, Schroeder RM, Malfatti CF. The influence of calcareous deposits on hydrogen uptake and embrittlement of API 5CT P110 steel. Corros Sci. 2017;118:178-89. http://dx.doi.org/10.1016/j.corsci.2017.02.007.

24. Wang S, Wang L, Liu X, Bao M, Liu L, Wang X, et al. Influence of CO_2 and H_2S concentration on hydrogen permeation behavior of P110 steel. Int J Electrochem Sci. 2017;12(11):10317-37. http://dx.doi.org/10.20964/2017.11.29.

25. Devanathan MAV, Stachurski Z, Tompkins FC. The adsorption and diffusion of electrolytic hydrogen in palladium. Proc R Soc Lond A Math Phys Sci. 1962;270(1340):90-102. http://dx.doi.org/10.1098/rspa.1962.0205.

26. Oudriss A, Martin F, Feaugas X. Experimental techniques for dosage and detection of hydrogen. In: Blanc C, Aubert I, editors. Mechanics-microstructure-corrosion coupling. London: Elsevier; 2019. p. 245-68.

27. ASTM: American Society for Testing and Materials. ASTM G148-97 A: standard practice for evaluation of hydrogen uptake, permeation, and transport in metals by an electrochemical technique. West Conshohocken: ASTM; 2018. p. 1-10.

28. Cheng XY, Zhang HX. A new perspective on hydrogen diffusion and hydrogen embrittlement in low-alloy high strength steel. Corros Sci. 2020;174:108800. http://dx.doi.org/10.1016/j.corsci.2020.108800.

29. Wu D, Huang C, Zhang O, Zhao L, Li W, Jin X. Investigation of hydrogen diffusion and trapping behavior under tensile stresses in a container steel. Mater Lett. 2019;256:126533. http://dx.doi.org/10.1016/j.matlet.2019.126533.

30. ISO: International Organization for Standardization. ISO EN. 17081 (Edition: 2014-28-02): method of measurement of hydrogen permeation and determination of hydrogen uptake and transport in metals by an electrochemical technique. Brussels: European Committee for Standardization; 2014.

31. Santos DS, Miranda PEV. The use of electrochemical hydrogen permeation techniques to detect hydride phase separation in amorphous metallic alloys. J Non-Cryst Solids. 1998;232-234:133-9. http://dx.doi.org/10.1016/S0022-3093(98)00487-6.

32. Yen SK, Huang IB. Critical hydrogen concentration for hydrogen-induced blistering on AISI 430 stainless steel. Mater Chem Phys. 2003;80(3):662-6. http://dx.doi.org/10.1016/S0254-0584(03)00084-1.

33. Chaudhari BS, Radhakrishnan TP. A reexamination of the trapping of hydrogen in iron and steel. Mater Trans, JIM. 1993;34(5):443-9. http://dx.doi.org/10.2320/matertrans1989.34.443.

34. McNabb A, Foster PK. A new analysis of the diffusion of hydrogen in iron and ferritic steels. Trans Metall Soc AIME. 1963;227:618-27.

35. Araújo DF, Vilar EO, Palma Carrasco J. A critical review of mathematical models used to determine the density of hydrogen trapping sites in steels and alloys. Int J Hydrogen Energy. 2014;39(23):12194-200. http://dx.doi.org/10.1016/j.ijhydene.2014.06.036.

36. Carrasco JP, Silva Diniz DD, Andrade Barbosa JM, Silva AA, Antonio dos Santos M. Numerical simulation of the hydrogen trapping effect on crack propagation in API 5CT P110 steel under cathodic overprotection. Int J Hydrogen Energy. 2019;44(5):3230-9. http://dx.doi.org/10.1016/j.ijhydene.2018.12.022.

37. Williamson GK, Hall WH. X-ray line broadening from filed aluminium and wolfram. Acta Metall. 1953;1(1):22-31. http://dx.doi.org/10.1016/0001-6160(53)90006-6.

38. Langford JI, Wilson AJC. Scherrer after sixty years: a survey and some new results in the determination of crystallite size. J Appl Cryst. 1978;11(2):102-13. http://dx.doi.org/10.1107/S0021889878012844.

39. Williamson GK, Smallman RE. III. Dislocation densities in some annealed and cold-worked metals from measurements on the X-ray debye-scherrer spectrum. Philos Mag. 1956;1(1):34-46. http://dx.doi.org/10.1080/14786435608238074.

40. Wang L, Cheng X, Peng H, Zhao PW, Cai Z. Effect of tempering temperature on hydrogen embrittlement in V-containing low alloy high strength steel. Mater Lett. 2021;302:130327. http://dx.doi.org/10.1016/j.matlet.2021.130327.

41. Merah N. DC potential drop calibration in creep-fatigue loading conditions. J Test Eval. 2000;28(4):301-6. http://dx.doi.org/10.1520/JTE12108J.

42. Pressouyre GM, Bernstein IM. A quantitative analysis of hydrogen trapping. Metall Trans, A, Phys Metall Mater Sci. 1978;9(11):1571-80. http://dx.doi.org/10.1007/BF02661939.

43. Zhang D, Gao X, Du Y, Du L, Wang H, Liu Z, et al. Effect of microstructure refinement on hydrogen-induced damage behavior of low alloy high strength steel for flexible riser. Mater Sci Eng A. 2019;765:138278. http://dx.doi.org/10.1016/j.msea.2019.138278.

44. Park GT, Koh SU, Jung HG, Kim KY. Effect of microstructure on the hydrogen trapping efficiency and hydrogen induced cracking of linepipe steel. Corros Sci. 2008;50(7):1865-71. http://dx.doi.org/10.1016/j.corsci.2008.03.007.

45. Bhadeshia HKDH. Prevention of hydrogen embrittlement in steels. ISIJ Int. 2016;56(1):24-36. http://dx.doi.org/10.2355/isijinternational.ISIJINT-2015-430.

46. Chu WY, Qiao LJ, Li JX, Su YJ, Yan Y, Bai Y, et al. Hydrogen embrittlement and stress corrosion cracking. Beijing. Science Press. 2013. p. 116-368.

47. Frappart S, Feaugas X, Creus J, Thebault F, Delattre L, Marchebois H. Study of the hydrogen diffusion and segregation into Fe–C–Mo martensitic HSLA steel using electrochemical permeation test. J Phys Chem Solids. 2010;71(10):1467-79. http://dx.doi.org/10.1016/j.jpcs.2010.07.017.

48. Zakroczymski T. Adaptation of the electrochemical permeation technique for studying entry, transport and trapping of hydrogen in metals. Electrochim Acta. 2006;51(11):2261-6. http://dx.doi.org/10.1016/j.electacta.2005.02.151.

49. Pressouyre GM. A classification of hydrogen traps in steel. Metall Trans, A, Phys Metall Mater Sci. 1979;10(10):1571-3. http://dx.doi.org/10.1007/BF02812023.

50. Wert CA, Frank RC. Trapping of interstitials in metals. Annu Rev Mater Sci. 1983;13(1):139-72. http://dx.doi.org/10.1146/annurev.ms.13.080183.001035.

51. Yazdipour N, Haq AJ, Muzaka K, Pereloma EV. 2D modelling of the effect of grain size on hydrogen diffusion in X70 steel. Comput Mater Sci. 2012;56:49-57. http://dx.doi.org/10.1016/j.commatsci.2012.01.003.

52. Li H, Venezuela J, Zhou Q, Shi Z, Yan M, Knibbe R, et al. Effect of shearing prestrain on the hydrogen embrittlement of 1180 MPa grade martensitic advanced high-strength steel. Corros Sci. 2022;199:110170. http://dx.doi.org/10.1016/j.corsci.2022.110170.

53. Stevens MF, Bernstein IM. Microstructural trapping effects on hydrogen induced cracking of a microalloyed steel. Metall Trans, A, Phys Metall Mater Sci. 1989;20(5):909-19. http://dx.doi.org/10.1007/BF02651657.

54. Li H, Venezuela J, Zhou Q, Shi Z, Dong F, Yan M, et al. Effect of cold deformation on the hydrogen permeation in a dual-phase advanced high-strength steel. Electrochim Acta. 2022;424:140619. http://dx.doi.org/10.1016/j.electacta.2022.140619.

55. Yang M. Microstructural characterization of quenched and tempered heat-treated P110 casing steels [thesis]. Edmonton: University of Alberta; 2021.

56. Lee J, Lee T, Mun D-J, Bae CM, Lee CS. Comparative study on the effects of Cr, V, and Mo carbides for hydrogen-embrittlement resistance of tempered martensitic steel. Sci Rep. 2019;9(1):5219. http://dx.doi.org/10.1038/s41598-019-41436-2.

57. Otsuka T, Hanada H, Nakashima H, Sakamoto K, Hayakawa M, Hashizume K, et al. Observation of hydrogen distribution around non-metallic inclusions in steels with tritium microautoradiography. Fus Sci Technol. 2005;48(1):708-11. http://dx.doi.org/10.13182/FST05-A1022.

58. Wei FG, Tsuzaki K. Quantitative analysis on hydrogen trapping of TiC particles in steel. Metall Mater Trans, A Phys Metall Mater Sci. 2006;37(2):331-53. http://dx.doi.org/10.1007/s11661-006-0004-3.

59. Lee HG, Lee J-Y. Hydrogen trapping by TiC particles in iron. Acta Metall. 1984;32(1):131-6. http://dx.doi.org/10.1016/0001-6160(84)90210-4.

60. Depover T, Verbeken K. Hydrogen trapping and hydrogen induced mechanical degradation in lab cast Fe-C-Cr alloys. Mater Sci Eng A. 2016;669:134-49. http://dx.doi.org/10.1016/j.msea.2016.05.018.

61. Cheng XY, Li H, Cheng XB. Carbides and possible hydrogen irreversible trapping sites in ultrahigh strength round steel. Micron. 2017;103:22-8. http://dx.doi.org/10.1016/j.micron.2017.09.005.

62. European Standard. EN BS 13173: cathodic protection for steel offshore floating structure. Czech Republic; 2001.

63. ISO: International Organization for Standardization. ISO 12473:2014 BE: general principles of cathodic protection in seawater. Geneva: ISO; 2014. 44 p.

64. Saastamoinen A, Kaijalainen A, Porter D, Suikkanen P, Yang J-R, Tsai Y-T. The effect of finish rolling temperature and tempering on the microstructure, mechanical properties and dislocation density of direct-quenched steel. Mater Charact. 2018;139:1-10. http://dx.doi.org/10.1016/j.matchar.2018.02.026.